

Banner appropriate to article type will appear here in typeset article

Linear Kelvin Wave Predictions in the $z \rightarrow 0$ Limit

Gabriel D. Weymouth

Ship Hydromechanics, Delft University of Technology, Delft, Netherlands

Corresponding author: G.D.Weymouth@tudelft.nl

(Received xx; revised xx; accepted xx)

Linear wave theory captures the essential physics of free-surface flows at a fraction of the computational cost of nonlinear and viscous methods, making it attractive for design, real-time control, and surrogate modeling applications. However, the Kelvin Green's function for a translating point-source generates unbounded wave energy in the $z \rightarrow 0$ limit, causing both numerical difficulties and physical inconsistencies. This paper develops a modified kernel for flat-ship theory incorporating an elliptic spanwise line integration that naturally resolves this ill-posedness, yielding finite wave energy over the entire free surface. We then present a fast evaluator for both point and line kernels using contour deformation adapted to the non-analytic Kelvin phase, achieving 10^4 - 10^5 speedup over direct quadrature while preserving the wake asymptotics. Predictions on the most challenging $z = 0$ limit demonstrate physically consistent wave patterns and wave resistance trends. An open-source Julia implementation is provided.

Key words: Kelvin waves, Green's function, numerical integration

1. Introduction

Linear potential theory for steady forward-speed wave problems captures the essential physics of ship-wave interaction at a tiny fraction of the computational cost of nonlinear and viscous solvers. This speed makes it attractive for applications such as design optimization, real-time control, and as the physics-informed backbone for machine learning surrogate models. However, the predictions also need to be free from empirical tuning parameters and robust for any input provided, which can be a problem for undamped potential flow.

The Kelvin Green's function for a steady translating disturbance exactly satisfies the linear free-surface boundary condition and has a well-established integral representation (Peters 1949; Noblesse 1981). For finite submergence, analytic and surrogate methods exist (Farell 1973; Newman 1987), but the elevation of the free surface is ill-posed as the source position moves up to the free surface, i.e., as $z \rightarrow 0^-$. The wave elevation spectrum $S_\zeta(k)$ peaks at $k^* \sim 1/|z|$ with amplitude $\sim 1/|z|$, diverging as $|z| \rightarrow 0$ and making the downstream wake unresolvable. Series and steepest-descent methods (Baar and Price 1988b; Iwashita and Ohkusu 1992; Doctors and Beck 1987) struggle with convergence,

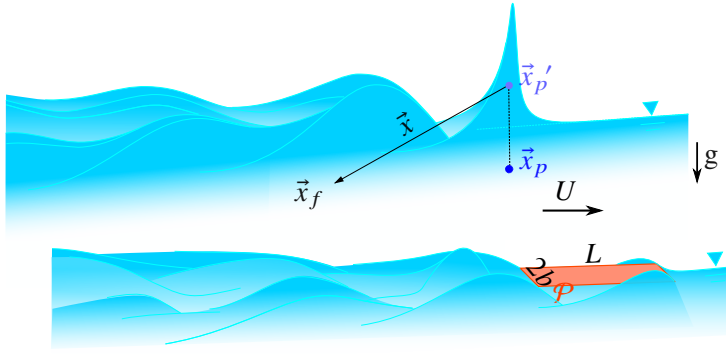


Figure 1. Schematic of the free surface prediction problem with submerged point source and flat-ship planform.

with stationary point coalescence, and with high wavenumbers in this limit. Recent contour deformation approaches (Deaño et al. 2018; Gibbs et al. 2024) are effective for analytic oscillatory integrands, but the Kelvin wavelike integral is non-analytic.

For surface-piercing bodies, the free-surface limit becomes unavoidable. The waterline contour contributes directly to the potential and must be evaluated at $z = 0$ (Baar and Price 1988a). Classic flat ship theory (Tuck 1975) prioritized practical prediction of wave resistance and hull pressure for high-speed, shallow-draft vessels, often using analytic or semi-analytic models and empirical corrections (e.g., spray) to match experiments, (Cole 1988). However, the singularity in the free-surface Green’s function at $z \rightarrow 0$ was not fully resolved, and direct evaluation of the waterline contribution remains problematic. The persistent difficulty of evaluating the free-surface Green’s function led to the development of the Neumann-Michell theory (Noblesse et al. 2013), which avoids evaluation on $z = 0$ using an implicit iterative scheme. Notably, Neumann-Michell theory was developed after the classic flat ship work, highlighting that the fundamental issues remain unresolved. This method sidesteps the $z \rightarrow 0$ singularity but sacrifices the directness and efficiency of explicit kernel representations.

This paper addresses the $z \rightarrow 0$ limit with an emphasis on obtaining meaningful finite energy free-surface predictions. The first contribution is analytical: Section 3 identifies the limiting wave elevation spectrum $S_\zeta(k^*) \sim 1/|z|$ stated above via stationary-phase analysis; Section 4 then develops a modified flat-ship model for $z \approx 0$, deriving the elliptic spanwise distribution of source strength that arises from the constant-downwash condition. The leading order flat-ship potential is the waterline contribution, but analytic integration replaces the divergent spectrum with a finite $S_\zeta(k) \sim 1/k^{3/2}$ even on $z = 0$. The second contribution is numerical: Section 5 develops a practical evaluator for both point and line kernels using contour deformation adapted to the non-analytic Kelvin phase, achieving 10^4 – 10^5 speedup over direct quadrature while preserving the wave energy. The new flat-ship theory is then used to study the wave elevation and wave drag generated by a rectangular planform on $z = 0$ as a function of the length and beam based Froude-number. An open-source Julia implementation is provided for reproducibility.

2. Kelvin Green’s Function for Linear Potential Flow

We consider steady, incompressible and irrotational flow in the half-space $z \leq 0$ with a reference frame translating in direction x at speed U , Figure 1. After scaling all lengths by the Kelvin length $\ell = U^2/g$ (where g is the gravitational acceleration) and the velocity potential ϕ by $U\ell$, that potential must satisfy $\nabla^2\phi = 0$ in the half-space and the linear

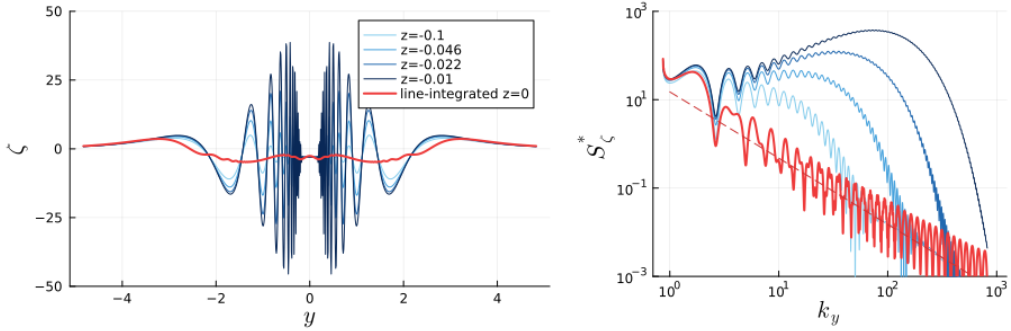


Figure 2. Free surface wave cut and spectra downstream of a unit point-source with $z \rightarrow 0$ and line-integrated source on $z = 0$. The wave cuts on the left are $\zeta(x = -8, y, z)$. The spectra on the right are $S_\zeta^* = |\zeta(x = -40, y(t_+), z)|^2$ evaluated along the divergent wave ridge, (3.2), with the carrier demodulated via Hilbert transform. The line-integrated results use half-beam $b = 1$ and $q_0 = \frac{2}{\pi}$ and the dashed line is the predicted $S_\zeta \sim k_y^{-3/2}$ decay.

free-surface boundary condition on the undisturbed free-surface plane

$$\partial_{xx}\phi + \partial_z\phi = 0 \quad \text{on} \quad z = 0$$

The well known Kelvin Green’s function of a translating point source at \vec{x}_p satisfies this boundary condition by construction, and is made up of near-field terms N which act close to the disturbance and a wavelike term W whose influence extends into the wake

$$G(\vec{x}_f, \vec{x}_p) = N(\vec{x}_f, \vec{x}_p) + W(\vec{x}_f - \vec{x}_p')$$

where \vec{x}_f is the field evaluation point and $\vec{x}_p' = (x_p, y_p, -z_p)$ is the image point reflected across $z = 0$. As in Noblesse et al. (2013), we have combined all of the near-field terms together, and fast surrogates are known for its efficient evaluation, such as in Newman (1987). In this work, we focus on the wavelike term.

Applying this Green’s function, the induced potential of a source-patch \mathcal{P} is

$$\phi(\vec{x}_f) = \iint_{\mathcal{P}} q(\vec{x}_p) G(\vec{x}_f, \vec{x}_p) \, da_p \tag{2.1}$$

where q is the source strength scaled by U . If \mathcal{P} lies on or near $z = 0$, then evaluating the linear free-surface elevation $\zeta = \partial_x\phi|_{z_f=0}$ and wave drag requires evaluating G , and in particular W , close to $z = 0$. In the next section, we show that this limit is singular for a point source even far downstream. This divergence is well known in practice, spurring developments such as Neumann-Michell theory, but we characterize it explicitly below as a basis for comparison.

3. Point-Source Singularity as $z \rightarrow 0$

We write the wavelike term in the general amplitude form

$$W_A(x, y, z) = 4H(-x) \int_{-\infty}^{\infty} A(t) \exp(z(1+t^2)) \sin(g(x, y, t)) \, dt \tag{3.1}$$

where $\vec{x} = (x, y, z)$ is the relative vector from the image, H is the Heaviside function that enforces the wake be downstream of the disturbance, and the phase is $g = (x + yt)\sqrt{1+t^2}$. The variable of integration is $t = \tan \theta$ where θ is the wave direction relative to x . For a

point-source the amplitude $A \equiv 1$, but this general form anticipates the analytic integration of Section 4 and gives a unified form for numerical evaluation in Section 5.

Stationary points of the wavelike phase satisfy $\partial_t g = 0$, and are given by

$$t_{\pm} = -\frac{x \pm \sqrt{x^2 - 8y^2}}{4y} \quad (3.2)$$

corresponding to the transverse and diverging wave systems inside the Kelvin wedge $y \leq \pm x/\sqrt{8}$. Near the centerline we have $|y/x| \rightarrow 0$ and therefore the diverging ridge goes to $t_+ \approx -x/2y \rightarrow \infty$. The stationary-phase estimate for the diverging wave contribution on $z = 0$ is

$$W(x, y, 0) \sim \frac{A_+}{\sqrt{\partial_{tt} g_+}} \sim \sqrt{\frac{t_+}{R}}, \quad \text{where } R = \sqrt{x^2 + y^2}$$

which grows without bound as $t_+ \rightarrow \infty$.

For finite submergence $z < 0$, exponential damping makes the diverging wave contribution to the wavelike elevation spectrum $S_{\zeta} = |\partial_x W|^2$ finite, but still unbounded in the limit. Defining $k_x = \sqrt{1 + t^2}$, $k_y = tk_x$ and $k = |\vec{k}| = 1 + t^2$; for large t_+ we have $k_x \approx |t_+|$ and $|k_y| \approx k \approx t_+^2$, and stationary phase analysis on the wave elevation spectrum gives

$$S_{\zeta}(k) \sim \left(k_x \exp(-|z|k) \left(\frac{t_+}{R} \right)^{1/2} \right)^2 \sim \frac{k}{R} \exp(-2|z|k) \quad (3.3)$$

where the k_x factor comes from differentiation by x . This spectrum peaks at

$$k^* = \frac{1}{2|z|}, \quad S_{\zeta}(k^*) \sim \frac{1}{R|z|}. \quad (3.4)$$

As $z \rightarrow 0$, the peak migrates to an arbitrarily high wavenumber with unbounded amplitude. This is not a local artifact: every point along the downstream wake is affected, with the amplitude only slowly modulated with R^{-1} . Figure 2 illustrates the unbounded growth as $z \rightarrow 0$ well downstream, in contrast with the regularized line-integrated kernel derived in the next section.

4. Line-Integrated Potential for Flat-Ship Theory

The singularity identified above motivates replacing the point-source kernel with an integrated Green's function. The flat-ship model provides a uniquely challenging setting as the entire planform rests on $z = 0$, Figure 1.

4.1. The Flat-Ship Model

Consider an extremely shallow-draft ship such as a flat-bottom planing hull with a small pitch angle α . In the limit $z_p \rightarrow 0^-$, the surface integral (2.1) that defines the potential reduces via Green's theorem and the linear free-surface boundary condition to a waterline contour integral around the planform boundary $\partial\mathcal{P}$ (Noblesse 1983; Baar and Price 1988a)

$$\phi(\vec{x}_f) = \oint_{\partial\mathcal{P}} q(\vec{x}_p) G(\vec{x}_f - \vec{x}_p) n_x \, dy_p.$$

For illustration, we focus on a rectangular planform of half-beam b and length L . As $n_x = \pm 1$ on the leading and trailing edges and zero on the sides, the potential on the

contour $\partial\mathcal{P}$ reduces to

$$\phi(\vec{x}_f) = \Delta_L \int_{-b}^b q(x_p, y_p) G(x_f - x_p, y_f - y_p, z_f) dy_p \quad (4.1)$$

where $\Delta_L f(x_p) = f(0) - f(L)$ is the difference across the bow and stern edges.

To determine the distribution of q , we impose a uniform downward velocity on the planform due to the small angle α

$$\partial_n \phi = \alpha, \quad (x_p, y_p) \in \mathcal{P}, \quad z_p \rightarrow 0^-.$$

Substituting $G = N + W$ into (4.1) and noting that W varies slowly compared to N on the planform, the dominant operator acting on q is the logarithmic near field term:

$$\int_{-b}^b q(y_p) \log |y - y_p| dy_p = \text{const}, \quad |y| < b.$$

This is precisely the classical constant-downwash integral equation of finite-wing theory, whose unique solution on $[-b, b]$ is the elliptic distribution

$$q(y_p) = q_0 \sqrt{1 - (y_p/b)^2}$$

with $q_0 \propto \alpha$. Using this elliptic distribution satisfies the velocity condition to leading order, neglecting the wavelike influence on the flat hull, as in classical thin-ship theory. As shown in the following, it also admits an exact integral representation that regularizes the wavelike function for all z .

4.2. The Line-Integrated Wavelike Kernel

We define the elliptically weighted spanwise integral of W as

$$\begin{aligned} W_b(x, y, z) &= \int_{-b}^b \sqrt{1 - (y_p/b)^2} W(x, y - y_p, z) dy_p \\ &= 4H(-x) \int_{-\infty}^{\infty} \exp(z(1+t^2)) \int_{-b}^b \sqrt{1 - \left(\frac{y_p}{b}\right)^2} \sin(g(x, y - y_p, t)) dy_p dt \end{aligned} \quad (4.2)$$

where we have swapped the order of integration. The inner integral is the Fourier transform of the elliptic distribution, which has the exact Bessel function representation

$$\int_{-1}^1 \sqrt{1 - \eta^2} e^{i\omega\eta} d\eta = \pi \frac{J_1(\omega)}{\omega}$$

where J_1 is the Bessel function of the first kind. Substituting $\eta = y_p/b$ and $\omega = bk_y$, W_b takes the general form (3.1) with amplitude A_b

$$A_b(t) = \pi \frac{J_1(b k_y(t))}{k_y(t)}. \quad (4.3)$$

The factor A_b is finite at $k_y = 0$ (with limit $\frac{1}{2}\pi b$) and decays as $k_y^{-3/2}$ for large k_y , filtering high wavenumber content even on $z = 0$. Applying the stationary-phase analysis of Section 3 with amplitude A_b at $z = 0$ gives the wave elevation spectrum

$$S_{b,\zeta}(k) \sim \frac{J_1^2(b k_y)}{k_y^2} \frac{k_y^{3/2}}{R} \sim \frac{1}{k_y^{3/2} b R}, \quad (4.4)$$

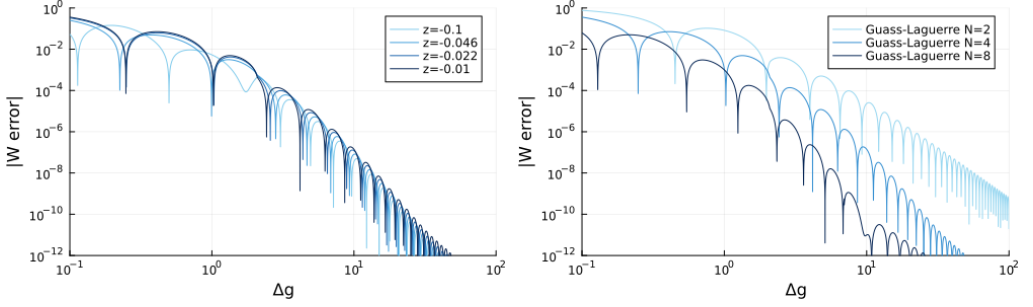


Figure 3. Error convergence of the partitioned quadrature method applied to $W(-8, y, z)$ on the same wavenuts in figure 2. Left shows the independence of the error as $z \rightarrow 0$ for $N = 4$ Gauss-Laguerre points, and right shows the trend with N for $z = -0.01$.

which is uniformly decaying and integrable, completely eliminating the unbounded high-wavenumber energy of the point-source kernel. This is demonstrated in Figure 2 for $b = 1$.

4.3. Wave Resistance

The wave spectrum leads directly to the flat-ship wave resistance D_W from the Havelock formula. Working in the variable $t = \tan \theta$ and using $k_x = \sqrt{1 + t^2} = \sec \theta$ we have

$$D_W = \frac{\rho}{\pi \ell^2} \int_{-\pi/2}^{\pi/2} |\mathbf{K}(\theta)|^2 \sec^3 \theta \, d\theta = \frac{\rho}{\pi \ell^2} \int_{-\infty}^{\infty} |\mathbf{K}(t)|^2 k_x(t) \, dt \quad (4.5)$$

where the Kochin function $\mathbf{K}(t)$ is the integral of the wavelike kernel over the planform. For the elliptic spanwise distribution and rectangular planform we have

$$\mathbf{K}(t) = q_0 U \ell^2 A_b(t) \Delta_L e^{ix_p k_x}.$$

Substituting into (4.5) and defining a resistance coefficient $C_W = D_W / (\rho U^2 b^2 \ell^2)$ gives

$$C_W = 4\pi q_0^2 \int_0^{\infty} A_w (1 - \cos(Lk_x)) \, dt, \quad A_w = \left(\frac{J_1(bk_y)}{bk_y} \right)^2 k_x, \quad (4.6)$$

The amplitude A_w is $O(1)$ at $t = 0$ and decays as t^{-5} for large t , so (4.6) is well-posed and rapidly convergent.

5. Partitioned evaluation method for wavelike kernels

Direct numerical quadrature and series expansions for the wavelike integral (3.1) are inefficient or even non-convergent as $z \rightarrow 0$. In this section, we detail an efficient and universally robust partitioned contour-deformation approach for the wavelike kernels, leveraging the classical stationary phase results above. An open-source Julia implementation is provided at Weymouth (2026).

5.1. Defining the saddle regions and quadrature methods

As in Gibbs et al. (2024), the wavelike integral is partitioned into two types of regions; (i) non-oscillatory intervals around stationary points, where standard quadrature is efficient, and (ii) the remaining semi-infinite tails, where complex contour quadratures converge exponentially. Unlike the analytic phase functions treated in Gibbs et al., the wavelike phase $g(x, y, t) = (x + yt)\sqrt{1 + t^2}$ is non-analytic and introduces branch points at $t = \pm i$.

y	absolute error	relative error	time (μs)	speedup	slowdown
0	3.78e-6	2.64e-7	30.4	6.59e4	7.02
0.5	1.16e-6	9.45e-8	34.3	1.77e5	6.45
0.9	1.14e-6	1.56e-7	131.7	7.86e4	26.6
1.1	2.09e-6	4.14e-7	149.5	1.20e5	29.4
1.35	2.75e-6	9.14e-7	57.4	6.22e5	11.6

Table 1. Error and timing of the partitioned quadrature approach applied to $W_b(-1, y, 0)$ for $b = 1$. Times measured on an Intel i9 laptop. Error and speed up are relative to an optimized adaptive Gauss-Kronrod quadrature method applied to W_b . Slowdown is relative to the partitioned quadrature applied to the point-source integral $W(-1, y, 0)$.

Therefore, we limit the non-oscillatory intervals to the real axis, defined such that each endpoint is separated from the stationary points t_{\pm} (3.2) by a prescribed phase increment Δg . Limiting the intervals to the real axis also simplifies locating the partition boundaries with numerical 1D root-finding.

The kernel is smooth over the non-oscillatory interval by construction, meaning direct quadrature can be applied efficiently. For this manuscript, we use adaptive Gauss-Kronrod quadrature to ensure a prescribed accuracy. The semi-infinite tails are evaluated using numerical steepest descent with Gauss-Laguerre quadrature on a complex contour emanating from the interval endpoints. The points along the complex contour are located by Newton’s method, selecting the $\sqrt{1 + t^2}$ branch such that the phase remains continuous along each contour. Outside the Kelvin wedge, a single pseudo-stationary point $t_0 = -x/4y = \Re(t_{\pm})$ is used, and the procedure is otherwise identical; this ensures continuity across the wedge boundary and the correct exponential decay in its vicinity.

Figure 3 shows the error of the point-source wavelike integral using this partitioning method. The error envelope is insensitive to \bar{x} , handling the transverse and diverging wave ridge merge as $y \rightarrow \pm x/\sqrt{8}$ and the energy growth as $z \rightarrow 0$ gracefully. The partition half-width Δg is the primary numerical parameter of the approach, encoding a tradeoff between the number of oscillations integrated along the real line and the exponential decay along the contours. If the contour starts too close to a stationary point (small Δg), the phase is slowly varying and the integrand decays slowly in the complex plane, requiring more Gauss-Laguerre points for accuracy. Conversely, large Δg ensures rapid decay and efficient contour quadrature, but increases the oscillations in the real-axis intervals, making them more expensive to integrate. The number of Gauss-Laguerre points N , is a secondary parameter: increasing N increases the error decay rate but also increases the length of the contours and computational expense. Herein, we set $\Delta g \approx 2\pi$ and $N = 4$, producing maximum errors around 10^{-6} with minimal computational cost.

5.2. Hankel function decomposition

The same contour-deformation strategy applies to the line-integrated source, extended to handle the additional oscillatory structure introduced by the Bessel function in A_b (4.3). To isolate these oscillations, the Bessel function is decomposed using Hankel functions away from $t = 0$

$$J_1(\omega) = \frac{1}{2} \left(\text{Hx}_1^{(1)}(\omega) e^{i\omega} + \text{Hx}_1^{(2)}(\omega) e^{-i\omega} \right) \quad (5.1)$$

where the scaled Hankel functions $\text{Hx}_1^{(1,2)}$ are slowly varying. The exponential factors oscillate at a frequency $\omega = bk_y$, but these can be absorbed into the wavelike phase,

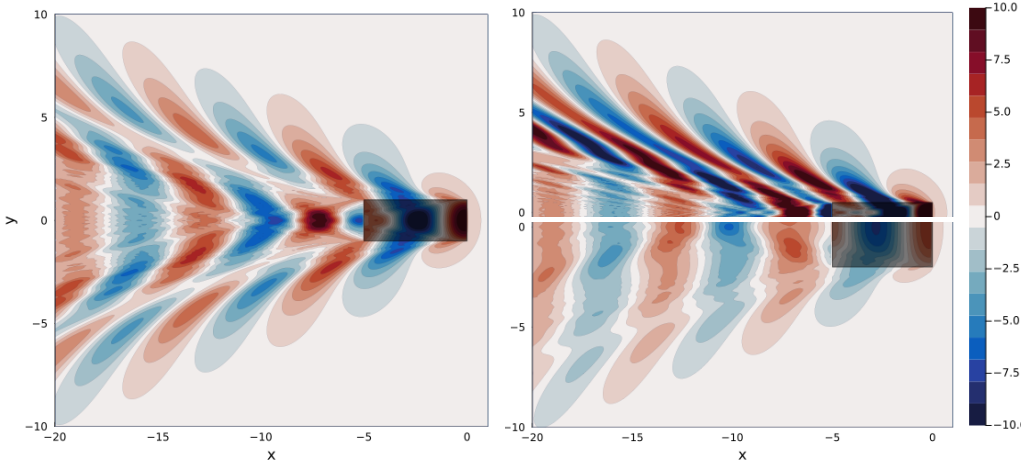


Figure 4. Flat-ship wave elevation ζ scaled by the spanwise integrated strength $\frac{\pi}{2}q_0b$ for $L = 5$. Left: full symmetric field for $b = 1$. Right: half-field for $b = 1/2$ (top) and $b = 2$ (bottom) using the same contour levels.

yielding two integrals with shifted phases $g(x, y \pm b, t)$. Each shifted phase has its own stationary points and associated non-oscillatory interval. The union of these intervals is integrated along the real line using the A_b prefactor. The union operator ensures that the contour starting points are sufficiently far from any stationary point, and these contours are computed twice, once for each Hankel function using its respective phase.¹

In general, the W_b quadrature requires approximately twice as many phase and kernel evaluations as W , and Bessel function evaluations are $O(10)$ times as expensive as simple trigonometric functions. However, the computational cost is still 10^4 – 10^5 faster than direct quadrature on $z = 0$ with relative errors less than 10^{-6} , Table 1.

6. Flat-ship wave predictions

Using the elliptic distribution, the flat-ship potential (4.1) becomes

$$\frac{\phi(\vec{x}_f)}{q_0} = \Delta_L W_b(x_f - x_p, y_f, z_f) + \Delta_L \int_{-b}^b \sqrt{1 - (y_p/b)^2} N(x_f - x_p, y_f - y_p, z_f) dy_p$$

where the near-field term N can be numerically integrated without issue and the wavelike term is calculated using the partitioned contour deformation method described in Section 5. Automatic Differentiation is used to evaluate the $\zeta = \partial_x \phi$ derivative.

Figure 4 shows a set of resulting flat-ship wave-fields for various b . First, we note that the predicted wave-elevations using the elliptic distribution have finite amplitudes and energy everywhere. Since submergence adds exponential wave damping, achieving finite energy at the flat-ship $z_p = 0$ limit guarantees well-behaved predictions for any submerged $z_p < 0$. In addition, the near-field contribution retains the expected logarithmic singularity across the line-source, resulting in a finite jump in ζ across the planform bow and stern edges. This discontinuity correctly represents the pressure jump across a zero-thickness flat ship and does not affect the far-field wave predictions.

¹The same approach can also be applied to the wave resistance integral (4.6). However, the faster $A_w \sim t^{-5}$ decay and slower $k_x \sim t$ phase function mean direct quadrature is also practical for that integral.

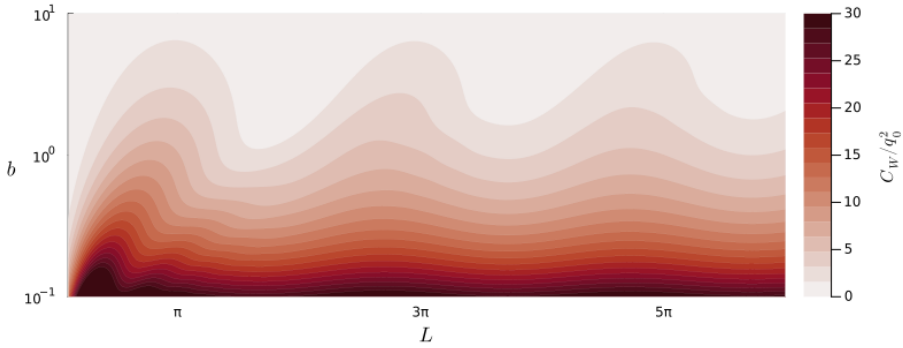


Figure 5. Flat ship wave resistance coefficient C_W scaled by q_0^2 as a function of the Kelvin-scaled planform length L and width b .

Second, the predictions capture many well-known physical patterns beyond the obvious Kelvin-wedge and wake shape. In particular, directly behind the planform we see that the interaction of the stern corner waves generates a large rooster-tail in the near wake, leaving a rough but low amplitude wave-field after the wave trains diverge in the far wake. The distinct waves generated by each corner of the planform also imply that the use of a smooth elliptical distribution has not artificially *rounded* the geometry.

The theory also predicts a strong decrease in the diverging wave elevation amplitude with increasing b for a given integrated line-source strength $\frac{\pi}{2}q_0b$. Intuitively, increasing the Kelvin-scaled beam b decreases the beam-based Froude number $F_b = b^{-1/2}$, taking the planform out of strong resonance with the Kelvin wavelengths $\lambda = 2\pi\ell \cos^2 \theta$. More specifically, as b increases, the continuous elliptic source distribution across the spanwise edges generates diverging waves with increasingly diverse spanwise phases, increasing the destructive interference. This mechanism is encoded in the Bessel function amplitude A_b (4.3) which filters high-wavenumber contributions more aggressively as b increases. In contrast, the transverse wave has $k_y \approx 0$ where $A_b \approx \frac{\pi}{2}b$, resulting in a roughly constant transverse amplitude after scaling by $\frac{\pi}{2}q_0b$.

Figure 5 plots scaled resistance (4.6) across a wide range of b, L . The interference factor $1 - \cos(Lk_x)$ produces classical constructive and destructive interference between the bow and stern wave systems, resulting in oscillating resistance values with L . More notably, the destructive spanwise interference discussed above results in a scaling $A_w \sim b^{-3}$ for large b and leads to a gradual but monotonic decrease in the resistance coefficient C_W with increasing b . This contrasts with classical thin-ship theory, which uses the beam-to-length ratio as a small parameter and predicts that wave resistance increases quadratically with beam. In flat-ship theory, the pitch angle α is the perturbation parameter while b is encoded in the Bessel function of the wavelike kernel, leading to the observed behavior of C_W .

7. Conclusions

The singularity in the point-source Kelvin Green's function as $z \rightarrow 0$ is fundamental, with the wave elevation spectrum diverging as $S_\zeta(k^*) \sim 1/|z|$ due to unbounded high-wavenumber energy. However, this singularity is not intrinsic to linear potential flow itself. The constant-downwash boundary condition on a flat-ship naturally produces an elliptic spanwise source distribution, and analytic integration of this distribution yields a regularized kernel with finite spectrum $S_\zeta(k) \sim k^{-3/2}$.

This resolution enables direct flat-ship predictions without empirical damping or iterative methods. Evaluations on $z = 0$ demonstrate physically consistent predictions, capturing wave interference patterns and realistic Froude number trends. Since $z = 0$ represents the most challenging limit, finite-energy predictions are guaranteed for all $z < 0$. The contour-deformation approach developed here evaluates both point and line kernels efficiently (10^4 – 10^5 speedup) for all \vec{x} , with potential applications in design optimization and machine learning surrogate models.

We note that the elliptic distribution developed here is merely the leading-order solution for flat planforms. Accounting for local hull geometry while retaining the regularized kernel framework is a natural extension. The approach could also be extended to time-varying source-strengths enabling direct calculation of the forward speed waterline contribution to ship motions in ocean waves.

REFERENCES

- J. J. M. Baar and W. G. Price. Developments in the calculation of the wavemaking resistance of ships. *Proceedings of the Royal Society of London. A. Mathematical and Physical Sciences*, 416(1850):115–147, Mar. 1988a. ISSN 0080-4630. .
- J. J. M. Baar and W. G. Price. Evaluation of the Wavelike Disturbance in the Kelvin Wave Source Potential. *Journal of Ship Research*, 32(01):44–53, Mar. 1988b. ISSN 0022-4502. .
- S. Cole. A simple example from flat-ship theory. *Journal of Fluid Mechanics*, 189:301–310, Apr. 1988. ISSN 1469-7645, 0022-1120. .
- A. Deaño, D. Huybrechs, and A. Iserles. *Computing Highly Oscillatory Integrals*. SIAM-Society for Industrial & Applied Mathematics, Philadelphia, 2018. ISBN 978-1-61197-511-6.
- L. J. Doctors and R. F. Beck. Convergence Properties of the Neumann-Kelvin Problem for a Submerged Body. *Journal of Ship Research*, 31(04):227–234, Dec. 1987. ISSN 0022-4502. .
- C. Farell. On the Wave Resistance of a Submerged Spheroid. *Journal of Ship Research*, 17(01):1–11, Mar. 1973. ISSN 0022-4502. .
- A. Gibbs, D. P. Hewett, and D. Huybrechs. Numerical evaluation of oscillatory integrals via automated steepest descent contour deformation. *Journal of Computational Physics*, 501:112787, Mar. 2024. ISSN 0021-9991. .
- H. Iwashita and M. Ohkusu. The Green Function Method for Ship Motion at Forward Speed. 1992. URL <https://trid.trb.org/View/441133>.
- J. N. Newman. Evaluation of the Wave-Resistance Green Function: Part 1—The Double Integral. *Journal of Ship Research*, 31(02):79–90, June 1987. ISSN 0022-4502. .
- F. Noblesse. Alternative integral representations for the Green function of the theory of ship wave resistance. *Journal of Engineering Mathematics*, 15(4):241–265, Oct. 1981. ISSN 1573-2703. .
- F. Noblesse. A Slender-Ship Theory of Wave Resistance. *Journal of Ship Research*, 27(01):13–33, Mar. 1983. ISSN 0022-4502. .
- F. Noblesse, F. Huang, and C. Yang. The Neumann–Michell theory of ship waves. *Journal of Engineering Mathematics*, 79(1):51–71, Apr. 2013. ISSN 1573-2703. .
- A. S. Peters. A new treatment of the ship wave problem. *Communications on Pure and Applied Mathematics*, 2(2-3):123–148, 1949. ISSN 1097-0312. . eprint: <https://onlinelibrary.wiley.com/doi/pdf/10.1002/cpa.3160020202>.
- E. O. Tuck. Low-Aspect-Ratio Flat-Ship Theory. *Journal of Hydronautics*, 9(1):3–12, Jan. 1975. ISSN 0022-1716. .
- G. D. Weymouth. KelvinFlatShip, 2026. URL <https://github.com/weymouth/KelvinFlatShip>.